Motion-selective areas V5/MT and MST appear resistant to deterioration in choroideremia

NeuroImage: Clinical 38 (2023) 103384

Contents lists available at ScienceDirect

NeuroImage: Clinical

journal homepage: www.elsevier.com/locate/ynicl

Motion-selective areas V5/MT and MST appear resistant to deterioration in choroideremia

Edward H. Silson [a,1], Chris I. Baker [a], Tomas S. Aleman [b,c], Albert M. Maguire [b,c], Jean Bennett [b,c], Manzar Ashtari [b,c,d,*]

[a] Section on Learning and Plasticity, Laboratory of Brain and Cognition, National Institute of Mental Health, National Institutes of Health, Bethesda, MD, United States
[b] Center for Advanced Retinal and Ocular Therapeutics (CAROT), University of Pennsylvania, Philadelphia, PA, United States
[c] F.M. Kirby Center for Molecular Ophthalmology, Scheie Eye Institute, University of Pennsylvania, Philadelphia, PA, United States
[d] Department of Radiology, University of Pennsylvania, Philadelphia, PA, United States

A B S T R A C T

Choroideremia (CHM) is an X-linked recessive form of hereditary retinal degeneration, which preserves only small islands of central retinal tissue. Previously, we demonstrated the relationship between central vision and structure and population receptive fields (pRF) using functional magnetic resonance imaging (fMRI) in untreated CHM subjects. Here, we replicate and extend this work, providing a more in-depth analysis of the visual responses in a cohort of CHM subjects who participated in a retinal gene therapy clinical trial. fMRI was conducted in six CHM subjects and six age-matched healthy controls (HC's) while they viewed drifting contrast pattern stimuli monocularly. A single ~3-minute fMRI run was collected for each eye. Participants also underwent ophthalmic evaluations of visual acuity and static automatic perimetry (SAP). Consistent with our previous report, a single ~ 3 min fMRI run accurately characterized ophthalmic evaluations of visual function in most CHM subjects. In-depth analyses of the cortical distribution of pRF responses revealed that the motion-selective regions V5/MT and MST appear resistant to progressive retinal degenerations in CHM subjects. This effect was restricted to V5/MT and MST and was not present in either primary visual cortex (V1), motion-selective V3A or regions within the ventral visual pathway. Motion-selective areas V5/MT and MST appear to be resistant to the continuous detrimental impact of CHM. Such resilience appears selective to these areas and may be mediated by independent retina-V5/MT anatomical connections that bypass V1. We did not observe any significant impact of gene therapy.

1. Introduction

Functional magnetic resonance imaging (fMRI) has proved a powerful tool for assessing cortical visual function alongside clinical ophthalmic evaluations across diverse patient populations (Morland, 2015; Ritter, 2019; Castaldi, 2019; Prabhakaran, 2021). Previous reports have demonstrated strong correlations between fMRI and patients' clinical measures (Papanikolaou et al., 2014; Dilks et al., 2014; Baker et al., 2008; Baseler, 2011; Binda et al., 2013). Specifically, population receptive field (pRF) modelling (Papanikolaou et al., 2014) has highlighted the close correspondence between fMRI and clinical results in patients presenting with cortical lesions (Papanikolaou et al., 2014), macular degeneration (Dilks et al., 2014; Baker et al., 2008; Baseler, 2011); Leber's congenital amaurosis following retinal gene therapy (Ashtari et al., 2014) and choroideremia (CHM) (Silson, 2018).

Prior work from our group highlighted that the peculiar topography of the visual field and extent of the sensitivity loss in subjects with CHM could be well represented by the spatial distribution and strength of pRF estimates derived from a single ~ 3 min fMRI scan (Silson, 2018). Previous measurements obtained from subjects with CHM who were not candidates for retinal gene therapy highlighted the feasibility of using fMRI and pRF modelling to assess the impact of retinal interventions to restore vision, such as retinal gene therapy.

The current study was designed to replicate and extend our prior work (Silson, 2018) and measure the potential impact of retinal intervention in a group of subjects with CHM who underwent retinal gene therapy. Measurements were taken in a cohort of six subjects with molecularly confirmed CHM (Table 1) who received retinal gene therapy injections into a single eye and six age-matched normal sighted healthy controls. For subjects with CHM, pRF data were analyzed from each eye separately (Treated, Untreated) and at two timepoints (Year 1 and Year 2 post treatment). For controls, pRF data comprised of a single timepoint and were averaged across eyes. Importantly, the fMRI protocol for pRF acquisition was independent of the main retinal gene

* Corresponding author.
E-mail address: ashtari@pennmedicine.upenn.edu (M. Ashtari).
[1] Current affiliation: Department of Psychology, School of Philosophy, Psychology & Language Sciences, University of Edinburgh, Edinburgh EH8 9JZ, United Kingdom.

https://doi.org/10.1016/j.nicl.2023.103384
Received 12 July 2022; Received in revised form 7 March 2023; Accepted 20 March 2023
Available online 22 March 2023

Table 1
Clinical and Molecular Characteristics of Subjects with CHM.

CHM Subject ID	Age at Enrolment	*REPI* Mutation	Visual Acuity (ETDRS) RE	LE	Treated Eye
PN04	33	c.1663A > T	20/25	20/25	LE
PN05	50	Large exom 1 del.	20/40	20/20	RE
PN06	37	c.1327_1328delAT	20/25	20/25	LE
PN07	43	c.11446 > T	20/25	20/20	RE
PN08	26	c.1327_1328delAT	20/25	20/25	RE
PN11	39	c.940-2A > T	20/20	20/20	RE

therapy trial and was initiated at a later stage. As such, no baseline pRF data was available for comparison. To assess any impact of gene therapy, we therefore looked at differences between treated and untreated eyes and over time.

2. Materials and methods

2.1. Subjects

Six subjects with molecularly confirmed CHM **(see** Table 1**)** enrolled in an ongoing gene therapy clinical trial (www.ClinicalTrials.gov Identifier: NCT02341807) and six healthy control participants with normal ophthalmic examinations were included in this study. All CHM participants underwent comprehensive ophthalmic examinations. Informed consent was obtained from individual participants after explanation of the study procedures in compliance with the Declaration of Helsinki. The study consent form was approved both by the Children's Hospital of Philadelphia and the University of Pennsylvania Internal Review Boards.

2.2. Retinal structural and Functional measures

Achromatic, light-adapted standard static automatic perimetry (SAP) was performed with a modified system Humphrey Field Analyzer (HFA II-i; Carl Zeiss Meditec, Dublin, CA, USA) by using a conventional 10–2 testing protocol grid (200-ms duration, 0.45° diameter, achromatic stimuli). We applied the standard cut offs of < 33% false positives, <33% false negatives and < 20% fixation losses. We did not actively monitor fixation losses because we have evidence on microperimetry of stable foveal fixation in all patients. Retinal imaging was performed with a spectral-domain optical coherence tomography (SD-OCT; Spectralis; Heidelberg Engineering, Carlsbad, CA, USA) system. SD-OCT was performed with 9-mm-long horizontal sections crossing the anatomical fovea **(see** Fig. 1**)**.

2.3. fMRI parameters

fMRI scans were conducted at the Children's Hospital of Philadelphia on a research-dedicated 3.0 T Siemens Verio system (Erlangen, Germany) using a 12-channel head coil. All scans were performed by a single operator and monitored to be free of artifacts at the time of acquisition.

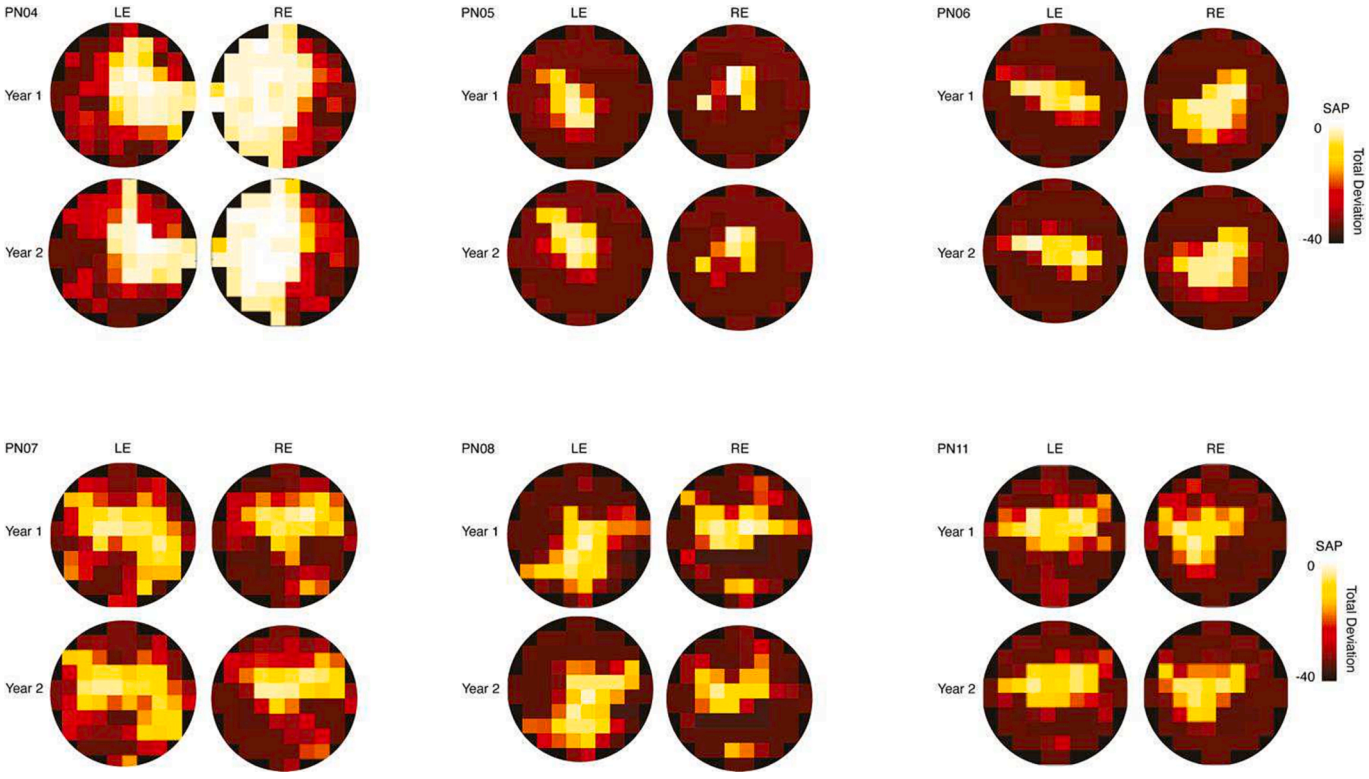

Fig. 1. Static automatic perimetry (SAP) measurements in subjects with CHM. Heat maps represent the total deviation SAP measurements for both the left-eye (LE) and right-eye (RE) of each subject with CHM and across both time-points (Year 1, Year 2). In these plots, bright cells (yellow/white) represent locations in the visual field with sensitivity either equal to or greater than normal age-matched controls, whereas dark cells represent locations in the visual field with decreased sensitivity relative to normal age-matched controls. SAP measurements in each eye are highly stable in each subject with CHM over time, suggesting very limited (if any) change in ophthalmic evaluation during this period. (For interpretation of the references to color in this figure legend, the reader is referred to the web version of this article.). (For interpretation of the references to color in this figure legend, the reader is referred to the web version of this article.)

2.4. pRF image acquisition

pRF experiments were performed using a blood-oxygenation-level-dependent (BOLD) sequence, acquiring 100 volumes with 29 slices at 2.8 × 2.8 × 2.5-mm resolution (matrix, 64 3 64; repetition time [TR]/echo time [TE], 2000/30 ms; flip angle, 90°; field of view, 180 mm^2 with total acquisition time of 3:24 min) in oblique orientation perpendicular to the calcarine sulcus. Four brain volumes were acquired at the beginning of each fMRI experiment to allow reaching T1 equilibrium and were not used in the final analysis. pRF acquisitions were conducted using a real-time fMRI function to monitor subjects' motion in real time. Scans were terminated if a subject's motion in three translational and rotational directions reached 1 mm or 1°, respectively.

2.5. Anatomical acquisition

A 3-D magnetization prepared rapid acquisition gradient echo (MPRAGE) sequence was used to obtain high-resolution T1- weighted anatomic scans with the following characteristics: TR/TE, 2080/2.43 ms; bandwidth, 180 Hz/Px; matrix size, 256 × 256; field of view, 256 × 256 mm2; 192 axial slices; slice thickness, 1 mm; inversion time, 1200 ms, with flip angle, 9°; number of excitations, 1; echo spacing, 7.3; integrated parallel imaging techniques, 2; and a total scan time of 5.45 min.

2.6. pRF mapping stimulus

The pRF stimulus consisted of a bar within a circular aperture with 100% contrast drifting checkerboards traversing through the visual field. The bar stimuli made a total of 8 sweeps, with 12 evenly spaced steps per sweep (1 step/TR). Specifically, the order of eight sweeps for each run were as follows: (1) left – right, (2) bottom right – top left, (3) top – bottom, (4) bottom left – top right, (5) right – left, (6) top left – bottom right, (7) bottom – top, and (8) top right – bottom left. The last six bar positions on each of the four diagonal sweeps were occluded to allow for baseline estimation. Bar stimuli were contained within a circular aperture with a total diameter of 22.58°. Each participant completed two runs with either the left eye or right eye occluded. Occlusion was controlled electronically via an MRI-compatible goggle system (Resonance Technology VisuaStim goggles, Northridge, CA), which allowed stimuli to be presented to each eye separately. In each run, while performing the pRF experiments, participants fixated monocularly on a small circular disk that appeared in the center of their visual field and changed periodically in color between red and green. To ensure their central fixation and attention to the experiment, subjects were asked to respond every time the small circular disk in the center changed color by using an MRI compatible response device.

2.7. pRF data preprocessing

All pRF data were analysed using the Analysis of Functional NeuroImages (AFNI) software package (Cox, 1996) (provided in the public domain by the National Institutes of Health, Bethesda, MD, USA; http://afni.nimh.nih.gov/afni). Images were preprocessed to control for subject motion (3dvolreg) by using the first volume of the first run as a reference, after removing the first four volumes to establish equilibrium. After motion correction, images were detrended (3dDetrend, removing second-order polynomial trends). fMRI images were slice-time corrected and aligned to participant-specific T1-weighted anatomical scans before projecting data onto participant-specific surface reconstructions (see below). No spatial smoothing was applied.

2.8. pRF data processing

All pRF analyses were conducted using a pRF implementation for the AFNI distribution (Cox, 1996; Silson et al., 2015). For every voxel in the brain, the model initially estimates the center of the pRF on an ×, y grid with 200 samples across both the height and width of the field of view (FOV). For each point in the grid, the sizes of pRFs (sigma) are sampled at the same resolution but over a default range of 0 to half the FOV (sampled at 100 even intervals). These default parameters result in four million possible pRFs (with unique ×, y location and size). Given the position of the stimulus in the visual field at every TR, the estimated time series for a receptive field of a given location and size is modelled. The model then makes use of a 2-D stimulus time series, which contains binary masks of the stimulus location at each TR and a convolution with a standard hemodynamic response function to produce four million predicted time series. Both Simplex and Powell optimization algorithms are used simultaneously to find the best time series/parameter sets (x, y, and size [sigma]) by minimising the least-squares error of the predicted time series measured against the acquired time series in each voxel. The model outputs for each voxel include the estimated diameter for the pRFs (size/sigma), along with the ×, y locations representing the pRF centre, and the corresponding explained variance (R^2) for the fit, which can be used to statistically threshold these data.

2.9. Visual field coverage

The visual field coverage maps were computed individually for all participants (CHM subjects and controls). These maps were derived from all voxels with an explained variance > 20% ($R^2 > 0.2$), irrespective of the voxels anatomical location within the brain. Each voxel's pRF was plotted as a scaled 2-D Gaussian onto a matrix representing the visual field. Once all pRFs were overlaid, the maximum explained variance (across voxels) was calculated for every position in the visual field (pixel of the matrix) (Prabhakaran, 2021; Winawer et al., 2010; Carvalho, 2021). The visual field was then divided into a 10x10 grid to match the positions sampled during ophthalmic evaluations (SAP).

2.10. Surface reconstructions

Surface reconstructions of the gray and white matter boundary of individual hemispheres for each participant were made using the Freesurfer4 (Fischl, 2012) autorecon script (provided in the public domain, https://surfer.nmr.mgh.harvard.edu/) and visualized using the Surface Mapping module of the AFNI (SUMA) software package (Saad and Reynolds, 2012).

2.11. Probabilistic retinotopic atlas

A publicly available probabilistic atlas of retinotopic maps (Wang et al., 2015) was used to define regions of interest (V1, V5/MT-MST, V4, VO1 & VO2) for pRF analyses. The atlas, derived from retinotopic mapping experiments in 55 individuals, provides the probability that a given cortical location falls within the boundary of each retinotopic map. For each ROI we selected a threshold of 30% of the maximum probability within the selected ROI.

2.12. Statistical analyses

Statistics were calculated using the R Studio package (version 1.3.9). Tests for potential effects of treatment (Treated versus Untreated) and time (1 Year versus Year 2) within subjects with CHM were performed using 3-way repeated-measures Analysis of Variance (rm-ANOVA). Comparisons between CHM subjects and controls were made using mixed-ANOVA models.

3. Results

Here, we focused on six subjects with CHM in whom both ophthalmic evaluation (using static automatic perimetry, SAP) and pRF data were collected at 1 Year and 2 Years post treatment. Our primary goal was to

confirm the positive relationship between ophthalmic evaluation of visual function and measurements of visual sensitivity derived from pRF modelling. A secondary goal was to assess any impact of retinal gene therapy on our pRF derived measurements of visual sensitivity. A tertiary goal was to quantify the apparent resilience of V5/MT and MST in CHM subjects. Importantly, this tertiary goal was post-hoc following our detailed analysis of the cortical topography of pRF responses. We report the results in chronological order below.

3.1. Correlations between SAP and pRF

Initially, we sought to replicate and extend our prior work (Silson, 2018) on the relationship between ophthalmic evaluation of visual function (via SAP) and visual field coverage maps of visual sensitivity derived from pRF modelling (Silson, 2018; Carvalho, 2021). Visual field coverage maps were derived from all suprathreshold voxels ($R^2 > 0.2$) regardless of anatomical location. Fig. 2 depicts the SAP and pRF coverage plots as heat maps for an example subject with CHM, PN04 (Left eye, Year 1). Despite being derived from very different measurements, there is a clear topographical similarity between the two plots with both showing higher sensitivity (yellow/white cells) in the right visual field. The corresponding scatter plot confirms the positive relationship between the two measurements. In this subject, there is a significant ($p < 0.0001$) positive correlation (Pearson's $r = 0.74$) between the SAP and pRF measures.

The Pearson's correlation between SAP and pRF values were computed in all CHM subjects for each eye and timepoint (Year 1, Year 2) separately **(**Table 2**)**. Consistent with the example presented above and our prior work (Silson, 2018), significant positive correlations were observed for the majority of comparisons (21/24 comparisons, ~87.5%: 6 CHM subjects*2 eyes *2 timepoints = 24 total comparisons). Out of the three cases in which correlations were non-significant, all were from pRF sessions involving a treated eye. In addition, two out of three were from the Year 2 timepoint.

3.2. Distribution of pRF responses across the cortical surface

Having established significant correlations between visual field coverage maps and ophthalmic evaluations we next sought to conduct an in-depth analysis of the distribution of visual responses across the cortical surface - extending our prior work. We examined the spatial distribution of pRF responses (explained variance) across the cortical surface in CHM patients and controls. Results revealed a striking difference between CHM and control groups. In controls, robust responses were observed throughout early visual cortex (EVC: V1-V3) and beyond. In contrast, subjects with CHM showed relatively reduced responses within EVC, but preserved responses on the lateral surface of the brain in the approximate anatomical location of motion-selective V5/MT and MST (Wang et al., 2015; Dumoulin, 2000; Amano et al., 2009). Fig. 3**A-D** depicts the cortical distribution of pRF explained variance, polar angle, eccentricity and pRF size across medial and lateral views of the left hemisphere for a representative control (SC02, LE). The cortical distribution of pRF responses for all CHM subjects (LE, Year 1) across medial and lateral views of the left hemisphere are shown in Fig. 3**E** Whereas robust responses are present in SC02 throughout visual cortex **(**Fig. 3**A)**, both medially within EVC and beyond, responses in EVC are reduced in CHM subjects (Fig. 3**E)**. Indeed, responses appear more anterior than anticipated in CHM subjects (**see supplementary materials**). Moreover, responses are preserved in CHM subjects within a small cluster on the lateral surface in the approximate location of the ascending limb of the inferior temporal sulcus (AlITS) - an anatomical landmark identified as the location of motion-selective V5/MT - MST (Dumoulin, 2000). The apparent residual responses on the lateral surface of subjects with CHM despite the large reduction in response in early visual areas relative to controls prompted us to quantify whether subjects with CHM show preserved pRF responses in motion-selective V5/MT-MST relative to controls.

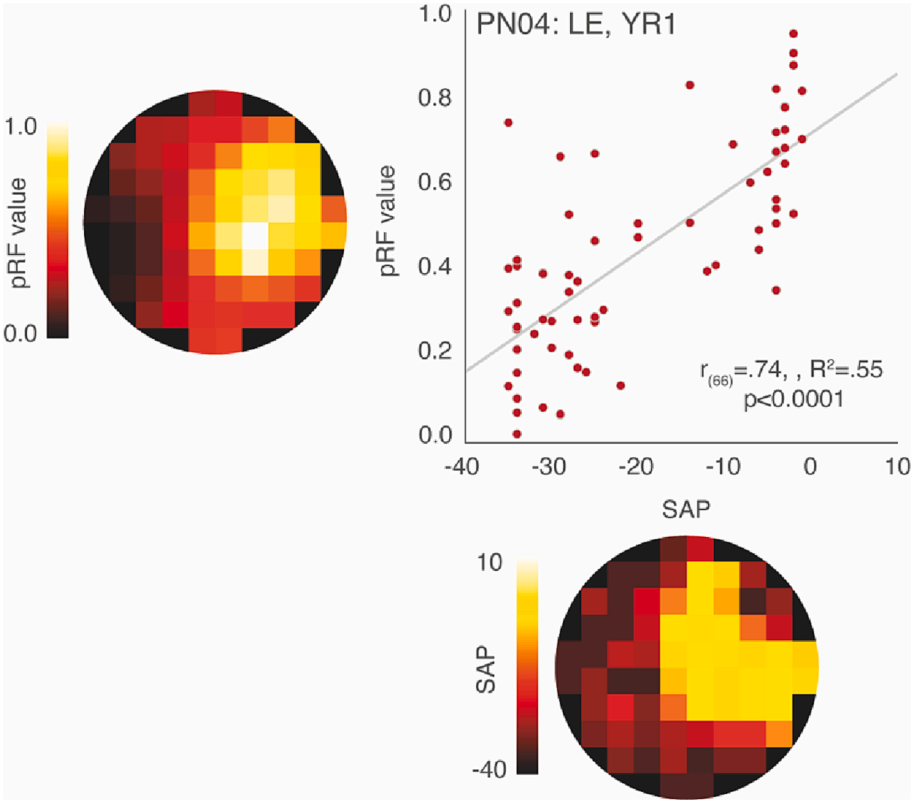

Fig. 2. Relationship between SAP and pRF-derived visual field coverage for an example CHM patient (PN04). The mean pRF values for each cell location is presented on the *y*-axis and the corresponding total deviation value, taken from the SAP measures, is shown on the *x*-axis. For ease of visual comparison, the calculated pRF and total deviation heat-maps are shown along the "Y" and "X" axes, respectively. The Pearson's correlations between these two measures are plotted for all 68 cells for the left eye 1 Year timepoint. A significant positive correlation was observed between the SAP and pRF measures ($r = 0.74$; $P < 0.0001$), demonstrating strong associations between the two measures of visual function in PN04.

Table 2
Pearson's correlation coefficients and corresponding p values between Clinical and pRF derived visual field coverage plots for all subjects with CHM. Data are shown for both the left and right eyes, Year 1 and Year 2 timepoints. Data for the treated eye are in bold for each CHM subject.

	Year 1				Year 2			
	Left Eye		Right Eye		Left Eye		Right Eye	
Patient ID	Pearson's *r*	*p* Value	Pearson's *r*	*p* Value	Pearson's *r*	*p* Value	Pearson's *r*	*p* Value
PN04	**0.742**	**<0.0001**	0.778	<0.0001	**0.714**	**<0.0001**	0.410	<0.001
PN05	0.758	<0.0001	**−0.082**	**ns**	0.529	<0.001	**0.075**	**ns**
PN06	**0.631**	**<0.0001**	0.484	<0.001	**0.730**	**<0.0001**	0.717	<0.001
PN07	0.621	<0.0001	**0.599**	**<0.001**	0.678	<0.0001	**0.767**	**<0.0001**
PN08	0.436	<0.001	**0.664**	**<0.0001**	0.579	<0.001	**0.455**	**<0.001**
PN11	0.584	<0.001	**0.459**	**<0.001**	0.702	<0.0001	**0.228**	**ns**

ns = $p > 0.05$

3.3. Preserved responses in V5/MT and MST in CHM

To quantify this apparent preservation, we utilized a freely available probabilistic atlas of retinotopic maps (Wang et al., 2015) to identify several regions of interest (ROIs): primary visual cortex (V1), a combined ROI of motion-selective V5/MT & MST on the lateral surface, a combined ventral ROI comprising V4, VO1/VO2 and motion-selective V3A **(**Fig. 4**)**. The inclusion of our ventral ROI (V4, VO1/VO2) serves as an important control as these regions occupy a similar position in the visual hierarchy (Wandell et al., 2007), but unlike V5/MT and MST are not thought to respond selectively to visual motion (Brewer, 2005). Additionally, combining V4, VO1/VO2 into a single ventral ROI also increased the number of included surface vertices to that approaching both V5/MT and MST and V1 (V1 = 1362, V5/MT & MST = 1013, V4 & VO1/VO2 = 980, & V3A = 1249).

We sought to test for any potential effect of treatment directly by comparing the data from the Treated versus Untreated eye within CHM subjects. Accordingly, for each CHM subject, we calculated the proportion of suprathreshold pRFs in each ROI (V1, V5/MT & MST, V4 & VO1/VO2) using an initial threshold of $R^2 > 0.15$, but results were found to be robust across multiple thresholds (**see supplementary materials**). ROIs were defined using 30% of the maximum probability, but importantly these results were largely identical across different probability thresholds (**see supplementary materials**). Overall, the patterns of pRF recruitment were largely stable within ROIs and across timepoints **(**Table 3**)**. These data were submitted to a 3-way rm-ANOVA with Eye (Treated, Untreated), ROI (V1, V5/MT & MST, V4 & VO1/VO2) and Time (1 Year, 2 Year) as within-subject factors. Neither the main effects of Eye ($F(1, 5) = 0.12$, $p = 0.73$), nor ROI ($F(2, 10) = 2.24$, $p = 0.15$), nor Time ($F(1, 5) = 0.003$, $p = 0.95$) were significant. Only the Eye × ROI interaction was significant ($F(2, 10) = 6.09$, $p = 0.01$) and all other interactions were not significant ($p > 0.15$). Given the non-significant effect of Time, we averaged these values across timepoints (Year 1, Year 2) to produce single estimates of the proportion of suprathreshold pRFs for each Eye and ROI, respectively. These values were then submitted to a two-way rm-ANOVA with Eye and ROI as within-subject factors (same levels as above). The main effect of Eye ($F(1, 5) = 6.24$, $p = 0.05$) approached significance, but the main effect of ROI ($F(2, 10) = 2.24$, $p = 0.15$) was not significant. These main effects were qualified however by a significant Eye × ROI interaction ($F(2, 10) = 6.09$, $p = 0.01$), which is driven by higher V1 proportions in the Untreated eye. A series of post-hoc paired t-tests revealed a significant difference between Eyes in V1 ($t(5) = 4.04$, $p = 0.01$), but neither V4 & VO1/VO2 ($t(5) = 0.83$, $p = 0.44$) nor V5/MT & MST ($t(5) = 1.27$, $p = 0.25$). Overall, these data did not reveal any indication of significant improvements in the treated over untreated eyes.

Having compared treated and untreated data directly within CHM subjects, we next turned to the question of whether the pattern of recruitment across ROIs was similar or different to that observed in the controls. We chose to compare the data from treated and untreated eyes with the controls separately, although highly similar results were obtained overall **(see** Table 3**)**. The pRF data for controls were averaged across the two eyes. These data revealed strikingly different activation patterns between the two groups. Overall, CHM subjects showed less than half the V1 recruitment as compared to controls for both treated and untreated eyes **(**Fig. 5**)**. This effect is entirely expected due to the nature of visual loss in CHM. The reduced recruitment relative to controls was also present within the ventral ROI (V4 & VO1/VO2), with CHM subjects again showing approximately half the level of recruitment relative to controls **(**Fig. 5**)**. In contrast, this pattern was not present for motion sensitive areas V5/MT & MST. Indeed, here CHM subjects on average exhibited either numerically higher levels of recruitment (in the Treated case) or equivalent levels (in the Untreated case) as compared to controls **(**Fig. 5**)**.

To quantify these data, a two-way mixed ANOVA with Group (CHM, controls) as a between-subject factor and ROI (V1, V5/MT & MST, V4 & VO1/VO2) as a within-subject factor was performed. Analyses were carried out separately for the Treated and Untreated eyes.

In the Treated case, both main effects of Group ($F(1, 10) = 22.31$, $p = 0.0008$) and ROI ($F(2, 20) = 6.39$, $p = 0.007$) were significant, which reflects on average the larger proportions in controls and differences across ROIs respectively. These were qualified however by a significant Group × ROI interaction ($F(2, 20) = 25.30$, $p = 0.000003$), which reflects the higher proportions for controls in both V1 and V4 &VO1/VO2, but largely equivalent proportions in V5/MT & MST for both groups. A series of post-hoc *t*-tests revealed a significant difference in ROI proportion between controls and CHM subjects in both V1 ($t(10) = 10.88$, $p = 0.0000007$) and V4& VO1/VO2 ($t(10) = 3.98$, $p = 0.002$), but importantly not in V5/MT & MST ($t(10) = 0.75$, $p = 0.47$).

A very similar pattern was observed when considering the data for the Untreated eyes relative to controls. Both main effects of Group ($F(1, 10) = 18.00$, $p = 0.002$) and ROI ($F(2, 20) = 10.98$, $p = 0.0006$) were significant, reflecting, on average, the larger proportions in controls and differences across ROIs, respectively. Again, these were qualified by a significant Group × ROI interaction ($F(2, 20) = 7.40$, $p = 0.004$), caused by proportions being higher for controls in both V1 and V4& VO1/VO2 ROIs, but largely equivalent for V5/MT & MST in CHM subjects. A series of post-hoc *t*-tests revealed significant differences in ROI proportion between controls and CHM subjects in both V1 ($t(10) = 5.63$, $p = 0.0002$) and V4 &VO1/VO2 ($t(10) = 3.15$, $p = 0.01$), but again, not for V5/MT & MST ($t(10) = 0.43$, $p = 0.67$).

3.4. No evidence for preserved responses in motion selective V3A

Along with the V5/MT and MST visual areas, V3A is considered the third motion-selective region in the human visual cortex, with its motion-selectivity being only slightly less than V5/MT and MST, respectively (McKeefry et al., 2008). Unlike V5/MT and MST, V3A is not thought to receive other direct retinal input independent of V1 (Sincich, 2004). To assess whether the preserved responses observed in V5/MT & MST might reflect this independent input the proportion of suprathreshold pRFs in V3A for each Eye (Treated and Untreated) were

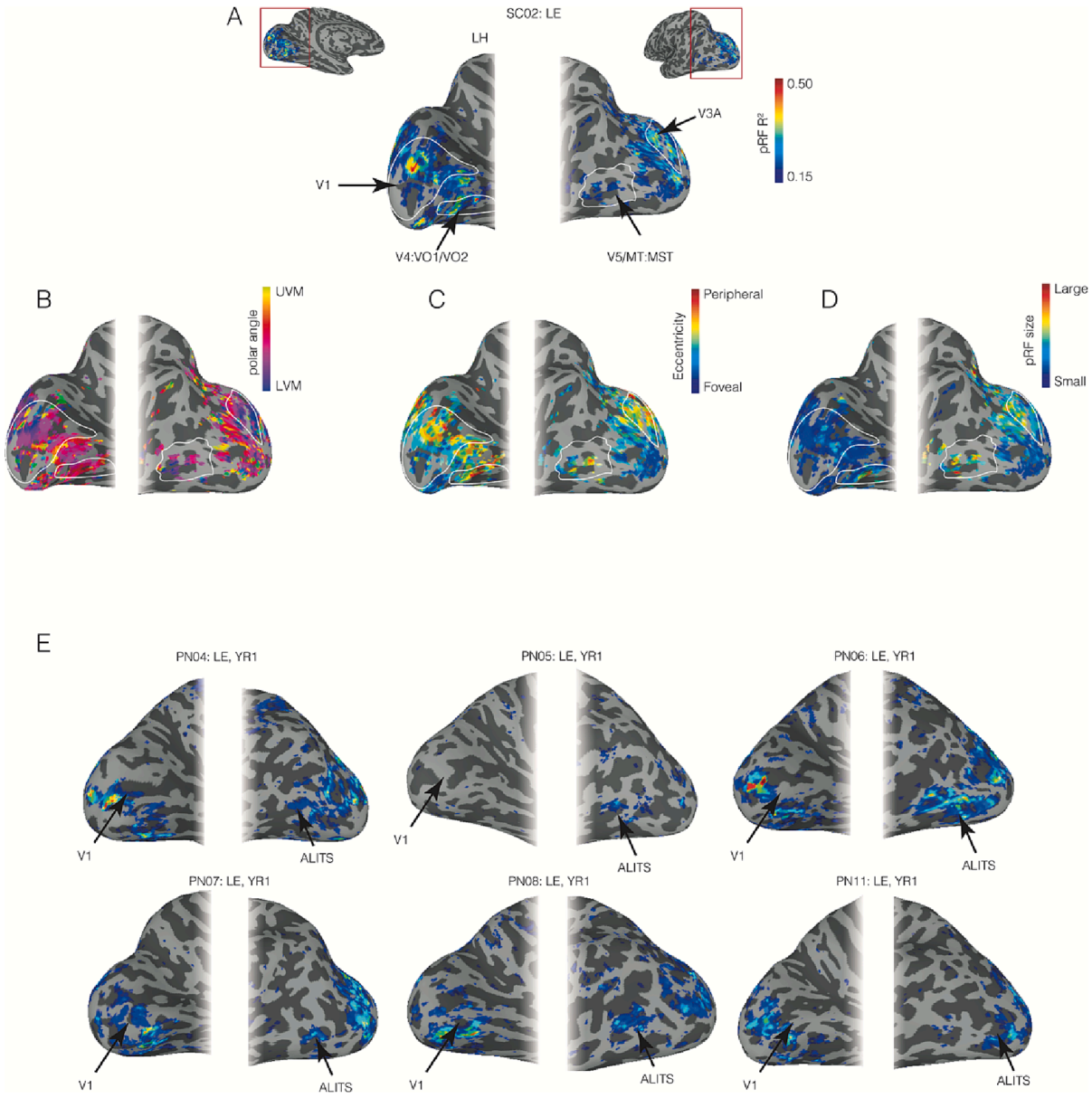

Fig. 3. Distribution of pRF explained variance, polar angle, eccentricity & pRF size from the left eye across the cortical surface of a representative healthy control (SC02) and distribution of pRF explained variance for all CHM subjects (LE, Year 1). A) Enlarged views of the posterior medial (Left image) and posterior lateral (Right image) cortical surfaces of the left hemisphere of SC02 are shown. Selected areas are shown in the red box and the full cortical surfaces are inset. These views represent partially inflated cortical surfaces (gyri = light gray, sulci = dark gray). The explained variance of the pRF model (derived from the left-eye run [LE]) is overlaid in false color (thresholded at $R^2 > 0.15$). As expected, robust responses are present throughout the early visual cortex (EVC) and beyond both medially and laterally. The borders of V1, V4:VO1/2, V5/MT:MST & V3A taken from a probabilistic atlas are shown in white. B) representation of polar angle in SC02. C) representation of eccentricity in SC02. D) representation of pRF size in SC02.E) Enlarged views of the posterior medial (Left image) and posterior lateral (Right image) cortical surfaces of the left hemisphere are shown for each CHM patient. For each CHM subject, the explained variance of the pRF model (derived from the left-eye run [LE], Year 1) is overlaid in false color. Unlike SC02, suprathreshold responses are relatively reduced in EVC, but are preserved within a small region on the lateral surface largely overlapping with the ascending limb of the inferior temporal sulcus (ALITS). (For interpretation of the references to color in this figure legend, the reader is referred to the web version of this article.). (For interpretation of the references to color in this figure legend, the reader is referred to the web version of this article.)

separately assessed using the same probabilistic retinotopic map atlas (Wang et al., 2015). Analyses showed significantly higher pRF proportions within V3A in controls as compared to the Treated eyes ($t(10) = 3.23$, $p = 0.008$). There was no significant difference between controls and the Untreated eyes ($t(10) = 1.87$, $p = 0.09$), although the data follow the same pattern as with the Treated eyes. A significant difference between Treated and Untreated eyes ($t(5) = 3.36$, $p = 0.02$), reflects lower proportions in the treated case. The significant drop in recruitment relative to controls observed in V3A (for the Treated eye) is more in line with the data from V1 and V4 & VO1/VO2 and not what was observed for V5/MT & MST.

3.5. pRF parameters stable across time in CHM

The analysis above focused on the area recruitment based on the variance explained of the pRF model. To assess whether treatment led to any changes in cortical organisation, over and above area recruitment we compared directly the average pRF centre locations (x, y) and pRF

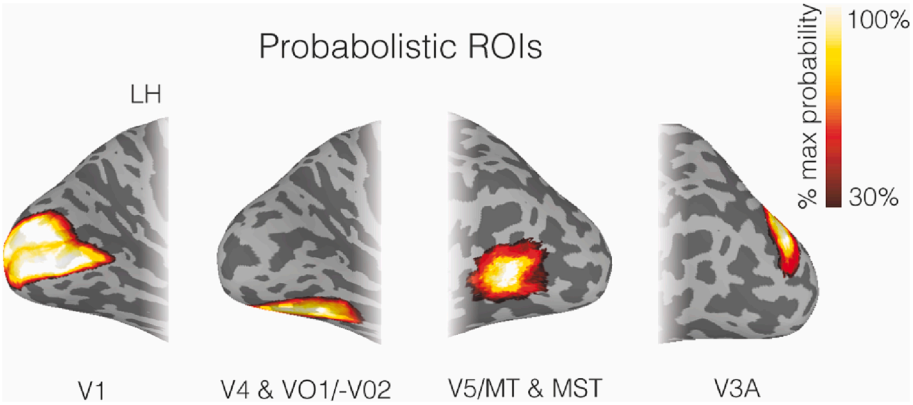

Fig. 4. Probabilistic ROI definitions. The location and extent of the probabilistic ROIs for V1, V4 & V01/V02, V5/MT & MST, and V3A are overlaid as heat maps onto enlarged views of the medial and lateral surfaces of the left hemisphere. For each ROI we selected all vertices with a probability > 30% of the maximum.

Table 3
Proportion of suprathreshold pRFs for each CHM subject, along with the mean and standard deviation across CHM subjects. Proportions are given for each eye (Treated, Untreated), ROI (V1, V4&VO1/VO2, V5/MT & MST) and Year (Year 1, Year 2).

	Year 1					
	V1		V4 & VO1/VO2		V5/MT & MST	
Patient ID	Treated	Untreated	Treated	Untreated	Treated	Untreated
PN04	0.148	0.370	0.155	0.183	0.205	0.194
PN05	0.019	0.010	0.023	0.014	0.145	0.106
PN06	0.382	0.323	0.341	0.241	0.469	0.398
PN07	0.095	0.286	0.093	0.160	0.300	0.299
PN08	0.145	0.215	0.245	0.177	0.630	0.402
PN11	0.095	0.288	0.128	0.253	0.134	0.032
Mean	0.147	0.249	0.164	0.171	0.314	0.239
STD	0.124	0.127	0.113	0.086	0.199	0.154
	Year 2					
	V1		V4 & VO1/VO2		V5/MT & MST	
Patient ID	Treated	Untreated	Treated	Untreated	Treated	Untreated
PN04	0.204	0.334	0.131	0.053	0.194	0.105
PN05	0.049	0.152	0.036	0.171	0.260	0.390
PN06	0.103	0.195	0.130	0.136	0.168	0.241
PN07	0.215	0.433	0.233	0.211	0.379	0.366
PN08	0.082	0.328	0.098	0.105	0.465	0.531
PN11	0.166	0.365	0.051	0.378	0.072	0.076
Mean	0.136	0.301	0.113	0.176	0.256	0.285
STD	0.068	0.107	0.071	0.113	0.144	0.177

size parameters in V1 and V5/MT & MST between year 1 and year 2 post treatment (for both treated and untreated eyes).

Across CHM participants, these parameters were very stable. Indeed, the absolute differences in pRF centre location and size between year 1 and year 2 were not significantly different from zero for either the treated or untreated eyes in V1 (t-tests versus zero; Treated: x, $t(5) = 2.00$, $p = 0.10$; y, $t(5) = 0.11, 0.91$; size, $t(5) = 0.46$, $p = 0.65$; Untreated: x, $t(5) = 0.91$, $p = 0.40$; y, $t(5) = 0.37, 0.72$; size, $t(5) = 0.27$, $p = 0.79$). In V5, although the absolute difference in × was marginally significant in the treated eye, the difference in y and size were not significant for either the treated or untreated eyes (t-tests versus zero; Treated: x, $t(5) = 2.82$, $p = 0.03$; y, $t(5) = 0.46, 0.66$; size, $t(5) = 0.15$, $p = 0.88$; Untreated: x, $t(5) = 0.83$, $p = 0.44$; y, $t(5) = 1.02, 0.35$; size, $t(5) = 0.67$, $p = 0.53$). Taken together these data suggest that pRF parameters remained largely unchanged as a function of either time or treatment.

4. Discussion

Consistent with our prior work (Silson, 2018), we demonstrated that the topography of the visual field and extent of the sensitivity loss in CHM subjects can be well represented by the spatial distribution and strength (i.e., explained variance) of pRF estimates derived from a single ~ 3 min fMRI scan. These data, along with other prior fMRI work (Papanikolaou et al., 2014; Dilks et al., 2014; Baker et al., 2008; Baseler, 2011; Ashtari et al., 2014; Silson, 2018; Ashtari et al., 2017; Morland, 2001) adds to the growing literature showing strong links between ophthalmic evaluations of visual function and those measured through fMRI and pRF modelling.

No significant improvement in visual functions were observed following retinal gene therapy as assessed through pRF modelling at one or two year post intervention. Indeed, the general pattern of the results was largely consistent across both Treated and Untreated eyes **(**Table 3 **&** Fig. 5**)**. The one exception being a difference in V1 recruitment at 2 Years post treatment with the Treated eyes showing a larger reduction. We also found no evidence for the impact of time post treatment in either the Treated or Untreated eyes for the time points examined here. The lack of impact of retinal gene therapy was also evident in the stability of the pRF parameters across time and treatment. Indeed, the lack of improvement following retinal gene therapy in our pRF measurements is consistent with preliminary findings from the clinical evaluation of the same group of CHM participants (Aleman et al., 2022). Here, Aleman and colleagues report no significant improvement of visual acuity relative to baseline, and moreover, report that measurements of

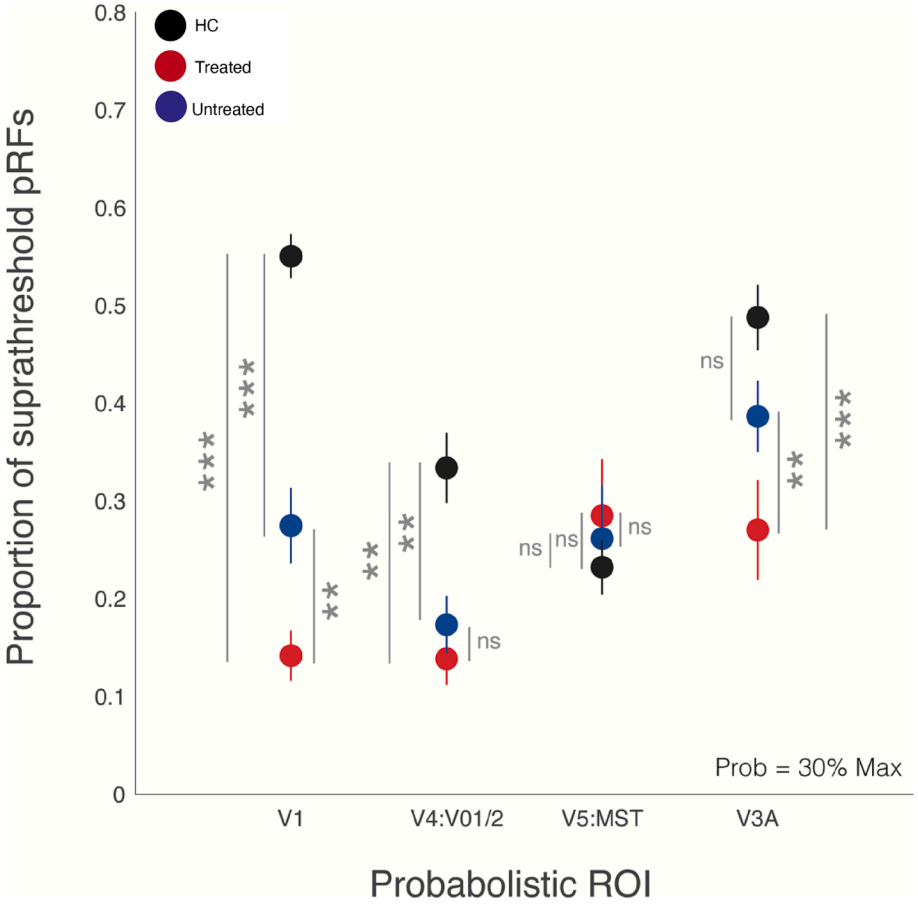

Fig. 5. Comparisons of the degree of cortical activation (area recruitment) during pRF mapping in V1, V4 & VO1/VO2 & V5/MT & MST & V3A ROIs for CHM subjects and healthy controls. Average proportion of suprathreshold pRFs for all ROIs are presented in black, red, and blue colors for HC's, treated and untreated eyes of CHM subjects respectively. For V1, CHM subjects show dramatic reductions in the level of pRF recruitment relative to HC's. The same reduction in activation pattern is repeated for V4 & VO1/VO2 and V3A (see additional V3A analyses below). In contrast, activation patterns within V5/MT & MST showed no statistical differences between HC's and CHM subjects. (For interpretation of the references to color in this figure legend, the reader is referred to the web version of this article.). (For interpretation of the references to color in this figure legend, the reader is referred to the web version of this article.)

visual sensitivity and rate of disease progression were not significantly different between eyes (treated, control). It is also important to note that our measurements reflect relatively long-term effects of retinal gene therapy (1 and 2 years post-treatment) as compared to any short-term effects that may have been present.

Examining the distribution of pRF data across the cortical surface in each CHM subject and control, revealed a striking and unanticipated feature of these data - the apparent resistance to deterioration of the V5-MST region in CHM subjects. Comparison of the proportion of suprathreshold pRFs between CHM subjects (at either Year 1 or Year 2) and controls showed no significant difference in the level of V5/MT & MST recruitment. In contrast, similar analyses for V1 showed around 50% reduction in V1 recruitment for CHM subjects as compared to controls. The large reduction in recruitment was also present in ventral control ROIs. The V4 & VO1/VO2 ROI was selected as a control non-motion sensitive region; it occupies a commensurate position within the visual hierarchy, but unlike V5/MT & MST does not exhibit motion sensitivity.

Since the pRF stimulus contained an object that was moving every 2 s and included drifting 100% contrast checkerboards within the moving bars, persistent activation in the motion sensitive V5/MT & MST area may be attributed to stimulus motion. To test this possibility, we analysed the proportion of suprathreshold pRFs in a different motion sensitive area (V3A) - a retinotopically organized area in close proximity to V5/MT & MST, which is also known to be motion sensitive (McKeefry et al., 2008; Strong et al., 20172017). pRF analyses for V3A showed a similar pattern of activation to that observed for V1 and V4 & VO1/VO2. CHM subjects showed a significant reduction in V3A recruitment (for the Treated eye) relative to controls, suggesting that resilience to deterioration (i.e., preserved level of activations) of the V5/MT & MST area as compared to controls is not simply due to either the motion-selective nature of these regions or the motion-information inherent in the stimulus.

The underlying mechanism for the apparent resilience of V5/MT and MST to the presence of retinal disease is largely unknown but could potentially reflect the anatomical connectivity and neuronal features of these regions. In addition to their well-established motion-selectivity (Zeki, 2004; Zeki, 1969; Anderson et al., 1998; Born and Bradley, 2005), V5/MT is also known to have rich cortical and subcortical connections (Sincich, 2004; Zeki, 2004; Felleman and Van Essen, 1991; Orban and Rockland, 1997), which are more heavily myelinated at birth than the surrounding cortex (Bourne and Rosa, 2006). For example, in new-world marmoset monkeys, V5/MT, unlike other extrastriate areas, shows adult-like patterns of cell maturity (Bourne and Rosa, 2006) similar to the primary sensory areas (e.g. V1 and A1) shortly after birth, leading some to classify this region as another primary visual area.

Anatomically, visual information is relayed to V5/MT from different sources. Direct inputs are established from the retina through retinopulvinar connections and via koniocellular cells (K-cells) of the lateral geniculate nucleus (LGN), as well as direct projections from V1 (Sincich, 2004; Nassi and Callaway, 2006; Nassi et al., 2006). Although the early maturation of V5/MT is thought to be due to the retinopulvinar projections and not those from V1. The balance of visual information received through these pathways depends on the stage of development or presence of retinal diseases, with the V1 afference dominating during postnatal period (Bourne and Rosa, 2006).

V5/MT's pattern of cortical and subcortical connections bypassing V1 offers a plausible mechanism for the apparent resistance to the reduced visual responsiveness present in CHM subjects. Indeed, a commensurate drop in pRF recruitment (like that observed in V4 &VO1/VO2 and V3A) would have been anticipated in V5/MT if the direct input from V1 constituted its sole source of visual information. Interestingly, one study (Sincich, 2004) identified a direct K-cell mediated thalamic

connection between LGN and V5/MT (Nassi et al., 2006). K-cells are considered to have similar temporal and spatial resolution as Magnocellular and Parvocellular cells and may contribute to vision information beyond motion sensitivity (Sincich, 2004; Eiber et al., 2018). It is possible therefore that the preserved responsiveness in V5/MT & MST of CHM subjects is mediated via this and other anatomical connections that bypass V1.

Despite sharing a foveal confluence, V5/MT and MST are known mainly for their large receptive fields and motion sensitivity, whereas V1 is more associated with small receptive fields and high-resolution vision. However, when central high-resolution vision is compromised, for example in macular degeneration, evidence suggests that peripheral visual areas can nevertheless maintain central visual function (Burnat, 2015). For example, substantial improvement in stereoacuity was observed following training in peripheral location in normally sighted individuals (Fendick and Westheimer, 1983; Westheimer, 2001). Further, improvements during crowding performed at the periphery have also been observed in patients after long term adaptation to macular degeneration (Chung, 2013). Other studies have also demonstrated the ability of peripheral vision to recognize natural scenes with fine spatial resolution when central viewing was artificially obscured (Larson and Loschky, 2009). Finally, inducing central retinal lesions in cats elicited similar permanent reductions in neuronal activity within V1-V4, but not V5/MT, which instead displayed an increase in neuronal activity (Burnat et al., 2017), suggesting that V5/MT can process more than just visual motion and take over visual functions typically processed by cortical regions more attuned to high-spatial processing.

An important distinction here is that these results were obtained either in normally sighted individuals or following lesions to the central retina. In contrast, CHM results in deterioration of the peripheral retina, leaving the central retina relatively unaffected. Despite this, clear reductions in cortical recruitment were evident throughout V1, including regions of V1 that represent the relatively intact central retina. The surprising finding here is that even under these circumstances, V5MT and MST appear resistant to such a reduction and can maintain visual responsiveness at a level commensurate with age-matched controls.

An important caveat of this work is that we did not collect additional fMRI or behavioural measurements of motion-sensitivity. Thus, it is possible that our pRF mapping stimulus was not optimized to drive responses in motion-selective regions. Future studies could use a more optimized stimulus and investigate whether the preserved responses in V5/MT & MST reported here are related to preserved visual functions such as motion discrimination threshold and contrast sensitivity.

Finally, it is worth noting that our analyses of area recruitment are based upon ROIs from a probabilistic atlas derived from healthy participants and not from CHM subjects, which could potentially bias the data in favour of the healthy controls. On the one hand, the higher recruitment within V1, V4:VO1/2 and V3A of the healthy controls could be attributed to the ROI definitions. On the other hand, area recruitment in V5/MT & MST were equivalent across groups, which cannot be simply explained by the ROI definitions.

5. Conclusion

Cortical areas V5/MT and MST appear resistant to deterioration in a cohort of confirmed CHM subjects. This effect was specific to these cortical areas and was not present in either V1, a ventral control ROI (V4 & VO1/VO2) or motion-selective V3A. Known independent anatomical connections from the retina to V5/MT crossing the LGN and pulvinar bypassing the V1 area may provide a plausible explanation for the preserved V5/MT responses. In addition, due to a slower degeneration of the V5/MT cells, there is a possibility that the coarse peripheral receptive fields are being recruited for fine spatial visual processing typically performed by central vision (Eiber et al., 2018). Finally, we replicated and extended our prior work (Silson, 2018) demonstrating a high correspondence between ophthalmic evaluations of visual function and those derived from a single ~ 3 min fMRI run. These data add to the growing body of literature demonstrating the utility of fMRI measurements to supplement existing clinical evaluations of visual function.

Declaration of Competing Interest

The authors declare that they have no known competing financial interests or personal relationships that could have appeared to influence the work reported in this paper.

Data availability

The authors do not have permission to share data.

References

Aleman, T.S., Huckfeldt, R.M., Serrano, L.W., Pearson, D.J., Vergilio, G.K., McCague, S., Marshall, K.A., Ashtari, M., Doan, T.M., Weigel-DiFranco, C.A., Biron, B.S., Wen, X.-H., Chung, D.C., Liu, E., Ferenchak, K., Morgan, J.I.W., Pierce, E.A., Eliott, D., Bennett, J., Comander, J., Maguire, A.M., 2022. Adeno-Associated Virus Serotype 2–hCHM Subretinal Delivery to the Macula in Choroideremia: Two-Year Interim Results of an Ongoing Phase I/II Gene Therapy Trial. Ophthalmology 129 (10), 1177–1191.

Amano, K., Wandell, B.A., Dumoulin, S.O., 2009. Visual Field Maps, Population Receptive Field Sizes, and Visual Field Coverage in the Human MT+ Complex. J. Neurophysiol. 102 (5), 2704–2718.

Anderson, J.C., Binzegger, T., Martin, K.A.C., Rockland, K.S., 1998. The Connection from Cortical Area V1 to V5: A Light and Electron Microscopic Study. J. Neurosci. 18 (24), 10525–10540.

Ashtari, M., Cyckowski, L., Yazdi, A., Viands, A., Marshall, K., Bókkon, I., Maguire, A., Bennett, J., Barnes, S., 2014. fMRI of Retina-Originated Phosphenes Experienced by Patients with Leber Congenital Amaurosis. PLoS ONE 9 (1), e86068.

Ashtari, M., Nikonova, E.S., Marshall, K.A., Young, G.J., Aravand, P., Pan, W., Ying, G.-S., Willett, A.E., Mahmoudian, M., Maguire, A.M., Bennett, J., 2017. The Role of the Human Visual Cortex in Assessment of the Long-Term Durability of Retinal Gene Therapy in Follow-on RPE65 Clinical Trial Patients. Ophthalmology 124 (6), 873–883.

Baker, C.I., Dilks, D.D., Peli, E., Kanwisher, N., 2008. Reorganization of visual processing in macular degeneration: Replication and clues about the role of foveal loss. Vision Res. 48 (18), 1910–1919.

Baseler, H.A., et al., 2011. Large-scale remapping of visual cortex is absent in adult humans with macular degeneration. Nat. Neurosci. 14, 649–655.

Binda, P., Thomas, J.M., Boynton, G.M., Fine, I., 2013. Minimizing biases in estimating the reorganization of human visual areas with BOLD retinotopic mapping. J. Vis. 13 (7), 13.

Born, R.T., Bradley, D.C., 2005. STRUCTURE AND FUNCTION OF VISUAL AREA MT. Annu. Rev. Neurosci. 28, 157–189.

Bourne, J.A., Rosa, M.G.P., 2006. Hierarchical Development of the Primate Visual Cortex, as Revealed by Neurofilament Immunoreactivity: Early Maturation of the Middle Temporal Area (MT). Cereb. Cortex 16, 405–414.

Brewer, A.A., et al., 2005. Visual field maps and stimulus selectivity in human ventral occipital cortex. Nat. Neurosci. 8, 1102–1109.

Burnat, K., 2015. Are Visual Peripheries Forever Young? Neural Plast. 2015, 1–13.

Burnat, K., Hu, T.-T., Kossut, M., Eysel, U.T., Arckens, L., 2017. Plasticity Beyond V1: Reinforcement of Motion Perception upon Binocular Central Retinal Lesions in Adulthood. J. Neurosci. 37 (37), 8989–8999.

Carvalho, J., et al., 2021. Visual Field Reconstruction Using fMRI-Based Techniques. Transl. Vis. Sci. Technol. 10, 25.

Castaldi, E., et al., 2019. Residual Visual Responses in Patients With Retinitis Pigmentosa Revealed by Functional Magnetic Resonance Imaging. Transl. Vis. Sci. Technol. 8, 44.

Chung, S.T.L., 2013. Cortical Reorganization after Long-Term Adaptation to Retinal Lesions in Humans. J. Neurosci. 33 (46), 18080–18086.

Cox, R.W., 1996. AFNI: Software for Analysis and Visualization of Functional Magnetic Resonance Neuroimages. Comput. Biomed. Res. 29, 162–173.

Dilks, D.D., Julian, J.B., Peli, E., Kanwisher, N., 2014. Reorganization of Visual Processing in Age-Related Macular Degeneration Depends on Foveal Loss. Optom. Vis. Sci. 91 (8), e199–e206.

Dumoulin, S.O., 2000. A New Anatomical Landmark for Reliable Identification of Human Area V5/MT: a Quantitative Analysis of Sulcal Patterning. Cereb. Cortex 10, 454–463.

Eiber, C.D., Rahman, A.S., Pietersen, A.N.J., Zeater, N., Dreher, B., Solomon, S.G., Martin, P.R., 2018. Receptive Field Properties of Koniocellular On/Off Neurons in the Lateral Geniculate Nucleus of Marmoset Monkeys. J. Neurosci. 38 (48), 10384–10398.

Felleman, D.J., Van Essen, D.C., 1991. Distributed Hierarchical Processing in the Primate Cerebral Cortex. Cereb. Cortex 1 (1), 1–47.

Fendick, M., Westheimer, G., 1983. Effects of practice and the separation of test targets on foveal and peripheral stereoacuity. Vision Res. 23 (2), 145–150.

Fischl, B., 2012. FreeSurfer. FreeSurfer. *NeuroImage* 62 (2), 774–781.

Larson, A.M., Loschky, L.C., 2009. The contributions of central versus peripheral vision to scene gist recognition. J. Vis. 9 (10), 6.
McKeefry, D.J., Burton, M.P., Vakrou, C., Barrett, B.T., Morland, A.B., 2008. Induced Deficits in Speed Perception by Transcranial Magnetic Stimulation of Human Cortical Areas V5/MT+ and V3A. J. Neurosci. 28 (27), 6848–6857.
Morland, A.B., et al., 2001. Abnormal retinotopic representations in human visual cortex revealed by fMRI. Acta Psychol. (Amst.) 107, 229–24727.
Morland, A.B., 2015. Organization of the Central Visual Pathways Following Field Defects Arising from Congenital, Inherited, and Acquired Eye Disease. Annu. Rev. Vis. Sci. 1, 329–350.
Nassi, J.J., Callaway, E.M., 2006. Multiple Circuits Relaying Primate Parallel Visual Pathways to the Middle Temporal Area. J. Neurosci. 26 (49), 12789–12798.
Nassi, J.J., Lyon, D.C., Callaway, E.M., 2006. The Parvocellular LGN Provides a Robust Disynaptic Input to the Visual Motion Area MT. Neuron 50 (2), 319–327.
Orban, G.A., 1997. Visual Processing in Macaque Area MT/V5 and Its Satellites (MSTd and MSTv). In: Rockland, K.S. (Ed.), *Extrastriate Cortex in Primates* 12. Springer, US, pp. 359–434.
Papanikolaou, A., Keliris, G.A., Papageorgiou, T.D., Shao, Y., Krapp, E., Papageorgiou, E., Stingl, K., Bruckmann, A., Schiefer, U., Logothetis, N.K., Smirnakis, S.M., 2014. Population receptive field analysis of the primary visual cortex complements perimetry in patients with homonymous visual field defects. Proc. Natl. Acad. Sci. 111 (16).
Prabhakaran, G.T., et al., 2021. Mapping Visual Field Defects With fMRI – Impact of Approach and Experimental Conditions. Front. Neurosci. 15, 745886.
Ritter, M., et al., 2019. Correspondence between retinotopic cortical mapping and conventional functional and morphological assessment of retinal disease. Br. J. Ophthalmol. 103, 208–215.
Saad, Z.S., Reynolds, R.C., 2012. SUMA. SUMA. *NeuroImage* 62 (2), 768–773.
Silson, E.H., et al., 2018. Comparing Clinical Perimetry and Population Receptive Field Measures in Patients with Choroideremia. Investig. Opthalmology Vis. Sci. 59, 3249.
Silson, E.H., Chan, A.- W.-Y., Reynolds, R.C., Kravitz, D.J., Baker, C.I., 2015. A Retinotopic Basis for the Division of High-Level Scene Processing between Lateral and Ventral Human Occipitotemporal Cortex. J. Neurosci. 35 (34), 11921–11935.
Sincich, L.C., et al., 2004. Bypassing V1: a direct geniculate input to area MT. Nat. Neurosci. 7, 1123–1128.
Strong, S.L., Silson, E.H., Gouws, A.D., Morland, A.B., McKeefry, D.J., 2017. A Direct Demonstration of Functional Differences between Subdivisions of Human V5/MT+. Cereb. Cortex 27 (1), 1–10.
Wandell, B.A., Dumoulin, S.O., Brewer, A.A., 2007. Visual Field Maps in Human Cortex. Neuron 56 (2), 366–383.
Wang, L., Mruczek, R.E.B., Arcaro, M.J., Kastner, S., 2015. Probabilistic Maps of Visual Topography in Human Cortex. Cereb. Cortex 25 (10), 3911–3931.
Westheimer, G., 2001. Is peripheral visual acuity susceptible to perceptual learning in the adult? Vision Res. 41, 47–52.
Winawer, J., Horiguchi, H., Sayres, R.A., Amano, K., Wandell, B.A., 2010. Mapping hV4 and ventral occipital cortex: The venous eclipse. J. Vis. 10 (5), 1.
Zeki, S.M., 1969. REPRESENTATION OF CENTRAL VISUAL FIELDS IN PRESTRIATE CORTEX OF MONKEY. Brain Res 14 (2), 271–291.
Zeki, S., 2004. Thirty years of a very special visual area, Area V5. J. Physiol. 557, 1–2.